

# Lateral Response Analysis of GRS Bridge Abutments under Passive Push

M. Ramalakshmi<sup>1</sup> and G. R. Dodagoudar<sup>2</sup>

<sup>1</sup>Department of Civil Engineering, IIT Madras, Chennai, India

<sup>2</sup>Department of Civil Engineering, IIT Madras, Chennai, India

E-mail: mrl.geotech@gmail.com

**ABSTRACT:** The objective of this study is to analyse the response of Geosynthetic Reinforced Soil (GRS) bridge abutments under lateral push towards the backfill. Hypoplastic constitutive model is adopted as the user defined material model in the subroutine, VUMAT, to represent the soil behaviour in finite element (FE) analysis. The unreinforced abutment and GRS abutments of eighteen different configurations are modelled using FE approach and analysed for static passive push. The passive force-displacement curves are obtained to study the lateral response of the GRS abutments. The inclusion of geogrid reduced the passive pressures behind the abutment wall. The GRS abutments with lesser geogrid spacing and longer geogrid reduced the passive pressures significantly compared to the other cases studied.

**Keywords:** GRS bridge abutment, Lateral response, Hypoplastic soil model, Static push, Passive earth pressure.

## 1. INTRODUCTION

During strong seismic shaking, the back-wall of the abutment is expected to break free of its base support and push into the backfill soil (Figure 1). The intrusion of the back-wall into the backfill is restricted by the passive force of the backfill soil. As a result, the backfill takes the earthquake induced inertial forces transmitted from the bridge superstructure through the abutment wall. The mechanism of passive force of bridge abutments in the longitudinal direction involves the abutment back-wall-soil interaction. Uncertainty in the passive load-displacement behaviour and evaluation of dynamic earth pressure during seismic excitation has motivated many large scale experimental and numerical investigations.

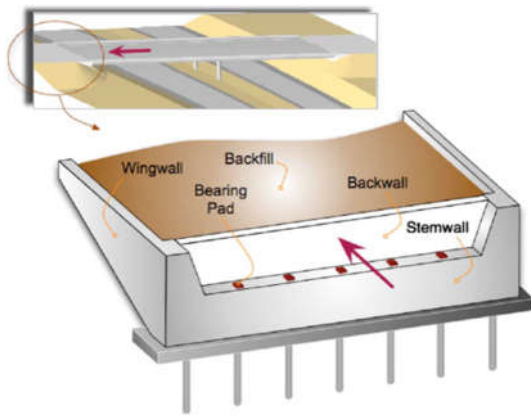


Figure 1 Typical seat type bridge abutment

Current seismic design procedures of structures are based on the force-displacement performance philosophy. The advent of performance-based design in engineering has evoked the need to compute the realistic force-displacement and moment-rotation relations for various types of civil engineering structures. The need for establishing the nonlinear lateral force-displacement (“pushover”) failure characteristics of foundations were indicated by National Earthquake Hazards Reduction Program (NEHRP) retrofit design guidelines of Federal Emergency Management Agency (FEMA 2000). The necessity to estimate the complete inelastic response of the abutment-soil system to progressively increasing lateral passive loads until failure has been felt by various researchers.

Studies on the development of passive force-displacement curves for bridge abutments have been carried out using both the analytical methods and several full scale tests. Full scale lateral load test on the bridge abutment of 1.67 m height was carried out by Stewart *et al.* (2007). Bozorgzadeh (2007) conducted experimental and numerical

analyses to examine the effect of backfill soil type, backfill height and vertical uplift of the abutment-wall on the lateral stiffness of the bridge abutments. Wilson (2009) and Wilson and Elgamal (2010) studied the behaviour of abutment wall under dynamic loads using finite element method (FEM). Rollins and Jessee (2013) studied the influence of skew angles of the bridge abutments on passive pressures through laboratory tests on the abutment walls with skew angles of 0°, 15°, 30° and 45°.

The problem of lateral response of abutment backfill system was approached through limit-equilibrium methods using logarithmic-spiral failure surfaces coupled with a modified hyperbolic soil stress-strain behaviour, called LSH (Logarithmic Spiral Hyperbolic) model (Shamsabadi *et al.* 2007, 2010). Equations for the hyperbolic force-displacement (HFD) curves were developed as an outcome of their study. The HFD relation is given as

$$P_p(u_H) = \frac{Cu_H}{1+Du_H} \quad (1)$$

where C and D are model constants and are given by

$$C = \left( 2K_{50} - \frac{P_{pmax}}{u_{H,max}} \right) \quad (2)$$

$$D = 2 \left( \frac{K_{50}}{P_{pmax}} - \frac{1}{u_{H,max}} \right) \quad (3)$$

where  $K_{50}$  is the average abutment stiffness and is obtained by  $P_{pmax} / (2 u_{H,50})$ ;  $P_{pmax}$  is the maximum passive force on the abutment;  $u_{H,50}$  is the displacement at  $P_{pmax}/2$ .

The GRS bridge abutment, due to its several advantages such as more adaptability to low quality backfill, easiness in construction and maintenance, minimized bump between the roadway and bridge, leads to an overall economy of the structure. Due to its multifold benefits, the GRS bridge abutment has now become a more common structure. The experimental and numerical investigations focusing on the evaluation of lateral passive capacity of the GRS bridge abutments would enhance the understanding of their seismic behaviour. The passive pressures behind the GRS abutments were evaluated by Fredrickson *et al.* (2017) through full scale lateral load tests on a 1.68 m high pile cap. A single layer of geogrid was provided near the mid height of the backfill. The inclusion of the geogrid in the backfill led to the reduction in initial tangent stiffness ( $K_i$ ) as well as the passive force ( $P_p$ ) behind the pile cap. The reduction in the maximum passive force was about 25%. However, more experimental and numerical studies are needed in order to evaluate the lateral passive capacity of the GRS bridge abutment systems under static and dynamic loadings so that they can be used in practical applications related to seismic response simulation of the bridge systems.

Several efforts have been made to analyse the vertical load-settlement characteristics of the GRS abutments. However, their lateral capacity also plays an important role during seismic excitation and the studies related to lateral capacity estimation are needed to be undertaken. In this study, the FE simulations are carried out to evaluate the lateral load-deformation characteristics of the unreinforced and GRS bridge abutments under static lateral passive loading conditions. Through hyperbolic fitting of the FE results, the HFD parameters for the GRS abutments are obtained. The HFD parameters are useful in the simplified seismic response analyses of bridge structures. Results of the study will be useful also in understanding the passive behaviour of GRS bridge abutment system under seismic excitation.

**2. SOIL CONSTITUTIVE MODEL**

The theory of elastoplasticity uses two geometrical surfaces namely the yield surface and plastic potential to determine the onset of plastic deformation and its direction. A material behaves elastically in the initial stage of deformation according to the theory of elastoplasticity. However, the granular and soft soils exhibit irreversible deformations from the beginning of the loading itself. This drawback of the elastoplastic theory has been overcome by the hypoplastic theory which describes the anelastic nature of the soil through a single equation (Kolymbas 2000), which remains same for both the loading and unloading processes. Since the difference between the loading and unloading is identified by the equation itself, it does not require a prior distinction between the elastic and inelastic displacements. Also it avoids the additional notions such as yield surface and plastic potential, making the constitutive model more realistic for the soils.

However, a few drawbacks were noticed when these hypoplastic models were used for cyclic stressing or deformation with small amplitudes (Bauer and Wu 1993). This shortcoming was due to the excessive accumulation of deformation, called ratcheting. In order to eliminate the ratcheting effects, Niemunis and Herle (1997) added the intergranular strain concept to the hypoplastic constitutive model proposed by von Wolffersdorff (1996). The additional state variable of intergranular strain represents the deformation of the interface layer between the grains. The hypoplastic constitutive model has greater potential and the same is used in the present study to model the backfill soil. For this purpose, the user defined material subroutine, VUMAT, is coded using FORTRAN and the same is linked with the FE code Abaqus 6.12 Explicit solver, to characterise the soil elements.

**3. VALIDATION OF VUMAT**

Full scale cyclic push test on the unreinforced bridge abutment was conducted at the University of California, Los Angeles (UCLA) to assess the lateral passive force of the abutments (Stewart *et al.* 2007, Lemnitzer *et al.* 2009). Figure 2a shows the configuration of the FE model developed for simulating the UCLA test. The abutment wall was 1.67 m high and 4.6 m long. This field test on the abutment wall has been simulated using Abaqus 6.12 in the present study to check the ability of the VUMAT to represent the backfill behaviour. The abutment soil in the field test was dense silty sand. The ranges of friction angle and cohesion of the soil were 39 - 40° and 14 - 24 kN/m<sup>2</sup> respectively. The hypoplastic parameters of the soil used in the FE modelling of the UCLA test are given in Table 1. The properties of the soil used in the UCLA test and the FE model are given in Table 2. Table 3 presents the material properties of the reinforced concrete abutment wall.

Four noded continuum plane strain elements, CPE4R, are used for the soil and abutment wall sections to simulate the plane strain conditions. Initially, the whole model is subjected to gravity loading to develop the initial stress conditions. Then the abutment is pushed towards the backfill with uniform horizontal displacement all along the full height, preventing the vertical uplift and rotation of the wall.

The same displacement cycle of pushing and pulling adopted in the field test was simulated in the FE simulation.

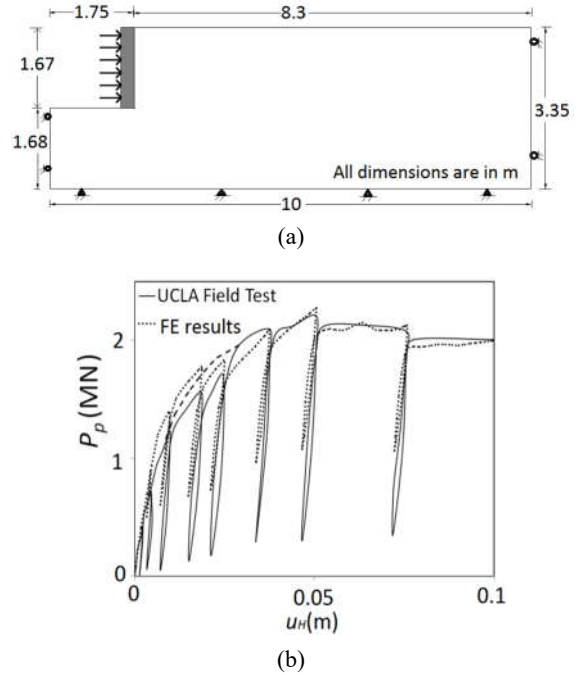


Figure 2 (a) Schematic of the UCLA test setup for FE simulation in the present study, (b) Passive force-displacement curves of UCLA test from field test results and FE results

Table 1 Hypoplastic parameters used for the soil (Niemunis and Herle 1997, Herle and Gudehus 1999)

$h_s$ (kPa)	$n$	$e_{d0}$	$e_{c0}$	$e_{i0}$	$\alpha$	$e$
2.6 <sup>e6</sup>	0.27	0.61	0.98	1.1	0.18	0.65
Intergranular strain parameters						
$\beta$	$R$	$m_R$	$m_T$	$\beta_r$	$\chi$	
1.1	1e <sup>-4</sup>	5.0	2.0	0.5	6	

Table 2 Properties of the backfill soil

FE model for	Unit weight, $\gamma$ (kN/m <sup>3</sup> )	Cohesion, $c$ (kN/m <sup>2</sup> )	Void ratio, $e$	Friction angle, $\phi_c$ (°)
UCLA test	20	24	0.61	35
Parametric study	20	0	0.65	30

Table 3 Material properties of abutment wall and geogrid reinforcement

Property	Abutment wall	Geogrid reinforcement
Elastic modulus (kPa)	23 x 10 <sup>6</sup>	1 x 10 <sup>3</sup>
Poisson's ratio	0.21	0.3
Density (kg/m <sup>3</sup> )	2400	1800

The passive force-displacement curve obtained from the present study is compared with that of the field test result in Figure 2b. The curve obtained from the field test has contained some irregularities due to the loss of vertical actuator control from 0.5 to 1 inch lateral displacement. The smoothed backbone curve of the experimental result is shown in thick dotted lines in Figure 2b. The capacity curve obtained from FE simulation coincides with the smoothed curve.

The maximum lateral capacity of the abutment-backfill system was measured to be 2210 kN (Lemnitzer *et al.* 2009) while the FE simulation yields a value of 2275 kN. The displacement at which the maximum force mobilised is about 50 mm in both the field test and FE analysis. This corresponds to the lateral displacement ( $u_H$ ) to abutment height ( $h$ ) ratio of 0.03. The residual capacity in the experiment was approximately 2033 kN, which was reached at a lateral displacement of 85 mm. In the FE studies, the passive capacity attains a residual state at the lateral displacement of 85 mm and it measures 1966 kN. The initial tangent stiffness ( $K_i$ ) values of the backbone curve are 34.5 and 36.6 MN/m respectively for the field test and FE analysis. Thus the present FE model is capable of assessing the passive behaviour accurately.

**4. FINITE ELEMENT MODELLING OF GRS ABUTMENTS**

In the present study, the GRS abutment-wall as shown in Figure 3 is used for the lateral response analysis. Since the objective of the study is to analyse only the lateral capacity of the backfill behind the abutment wall, only that region behind the abutment is modelled as the reinforced soil in the analysis. Figure 4 shows the distribution of reinforcement layers for the different GRS abutment models considered in the study.

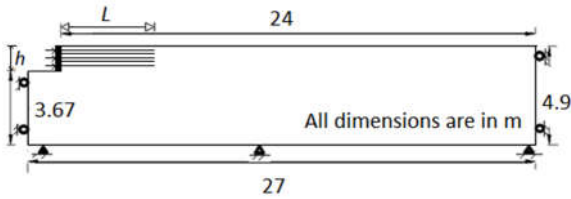


Figure 3 Model of the GRS abutment showing overall dimensions and boundary conditions

The region beneath the abutment has been assumed and modelled as unreinforced soil since the reinforcement (i.e. geogrid) beneath the bridge sill level may not influence the lateral force of the abutment-wall much. The backfill used for the study is sand and the Toyoura sand properties are assigned. The VUMAT has been developed as an user defined material model and uses the hypoplastic constitutive model to represent the soil continuum in the study. In the term  $L/h$  ratio,  $h$  is the height of the GRS abutment from the bridge sill level to the top surface of the backfill soil as shown in Figure 3. The distance between the abutment wall and the roller boundary placed behind the abutment wall is kept far away so that the boundary effects are negligible. The GRS abutment walls of heights 1.2 m and 2 m are considered in the analyses.

Totally eighteen different GRS abutment configurations with three different geogrid spacings ( $s$ ) and three different geogrid lengths ( $L$ ) are modelled and analysed. Figure 4 depicts the geogrid layouts for different GRS abutment configurations considered in the analyses. The geogrid spacings used in the study are 0.2 m, 0.4 m and 0.6 m. The GRS abutments with three different  $L/h$  ratios of 3, 4 and 5 are modelled to study their influence on the passive pressures. The geogrid reinforcement is modelled as an elastic material. The material properties used for the geogrid are given in Table 3. The reinforcements are modelled with truss elements, T2D2. The interfacial friction angle for the abutment-backfill interface and the geogrid-backfill interface is taken as 30°. The interface between the bottom of the abutment wall and the soil beneath is considered as frictionless.

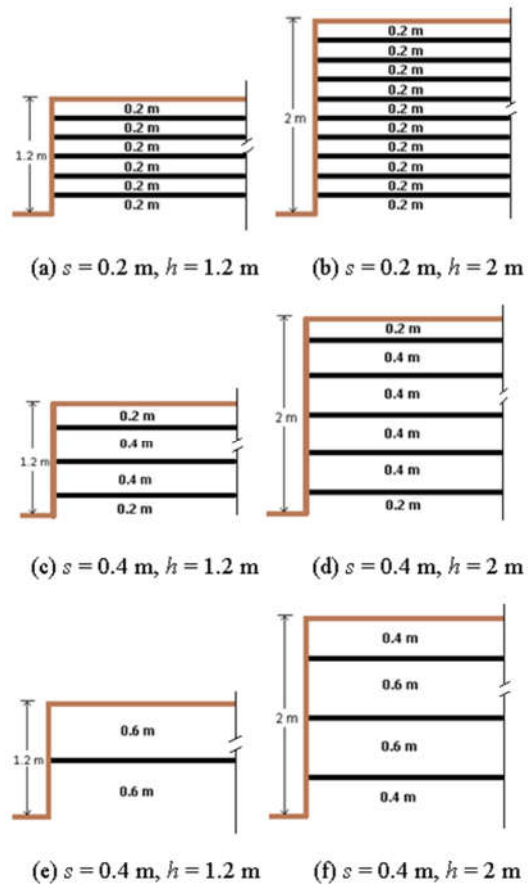


Figure 4 Different GRS abutment configurations considered in the analysis. (All dimensions are in m)

**5. GRS ABUTMENTS - FE RESULTS AND DISCUSSION**

**5.1 Passive force-displacement curves**

Figure 5 shows the variation of passive force,  $P_p$  with lateral displacement ratio ( $u_H/h$ ). The FE results are shown as scatter plots with hollow symbols. For the scatter plots, hyperbolic fits are established. The hyperbolic fits correspond to an  $u_{H,max}$  of 0.2  $h$ . The corresponding HFD parameters for the abutment of heights ( $h$ ) 1.2 m and 2 m are presented in Tables 4 and 5 respectively. The HFD response plots for the GRS abutments lie below that of the unreinforced abutment, thereby showing a significant influence of the geogrids on the passive force. Closely spaced and longer geogrids show more reduction in the passive force. The difference between the HFD parameters of the reinforced and unreinforced abutments is more for the case of higher abutments.

Table 4 HFD parameters for 1.2 m high abutment

$s$ (m)	$P_{pmax}$ (kN/m)				$K_{50}$ (kN/cm/m)			
	0.2	0.4	0.6	Mean	0.2	0.4	0.6	Mean
$L/h = 3$	281	287	320	<b>296</b>	138	179	246	<b>188</b>
$L/h = 4$	297	263	326	<b>295</b>	98	124	199	<b>140</b>
$L/h = 5$	267	277	327	<b>290</b>	115	192	202	<b>170</b>
Mean	<b>282</b>	<b>276</b>	<b>324</b>	<b>294</b>	<b>117</b>	<b>165</b>	<b>215</b>	<b>166</b>
Unrein	<b>331</b>				<b>229</b>			

Table 5 HFD parameters for 2 m high abutment

<i>s</i> (m)	$P_{pmax}$ (kN/m)				$K_{50}$ (kN/cm/m)			
	0.2	0.4	0.6	Mean	0.2	0.4	0.6	Mean
$L/h = 3$	545	530	511	<b>529</b>	213	276	340	<b>276</b>
$L/h = 4$	475	502	519	<b>499</b>	192	189	360	<b>247</b>
$L/h = 5$	370	462	565	<b>466</b>	661	592	513	<b>589</b>
Mean	<b>463</b>	<b>498</b>	<b>532</b>	<b>498</b>	<b>355</b>	<b>352</b>	<b>404</b>	<b>371</b>
Unrein	<b>648</b>				<b>598</b>			

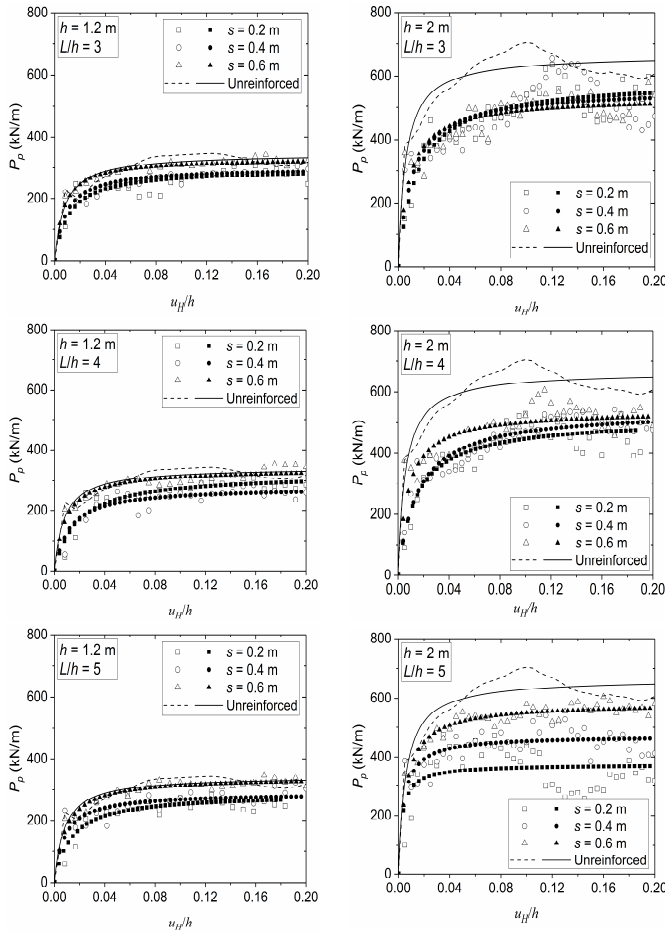


Figure 5 Variation of passive force  $P_p$  with  $L/h$  ratio

5.2 Initial tangent stiffness

It is seen from Figure 5 that the initial tangent stiffness,  $K_i$  values of the GRS abutments are different for each of the configurations studied. The initial tangent stiffness for the GRS abutments is less than that of the unreinforced abutment. The magnitudes of  $K_i$  of the GRS abutments of different configurations are given in Table 6.

Table 6 Initial tangent stiffness values of the GRS abutments of 2 m height

<i>s</i> (m)	$K_i$ (kN/cm/m)		
	0.2	0.4	0.6
$L/h = 3$	1438	1052	1687
$L/h = 4$	754	882	1590
$L/h = 5$	386	816	1590
Unreinforced	2353		

For the cases of higher abutments, the value of  $K_i$  decreased by a maximum factor of 0.84. It is also observed from Table 6 that the lesser geogrid spacing and larger  $L/h$  ratio decreased the  $K_i$  significantly.

5.3 Maximum passive force

In order to quantify the reduction in the value of maximum passive force a Reduction Factor ( $RF$ ) has been used in the present study. It is defined as

$$RF = \frac{P_{pmax,unrein} - P_{pmax,GRS}}{P_{pmax,unrein}} \quad (4)$$

In Figures 6a and 6b, the  $RF$  has been plotted against  $s$  and  $L/h$  respectively. In Figure 6a, most of the plots show continuously decreasing downward slope. The downward slope indicates the decrease of  $RF$  with increasing  $s$ . Similarly, in Figure 6b, the curves are either flat or show an upward slope, which means the increase of  $RF$  with  $L/h$ . In Figures 6a and 6b, the positions of the  $RF$  plots for 2 m high abutment are above the plots of the 1.2 m high abutment. It can be understood that the decrease of passive force is relatively more in the case of higher abutments and can be attributed to the increased number of geogrid layers in the higher abutments.

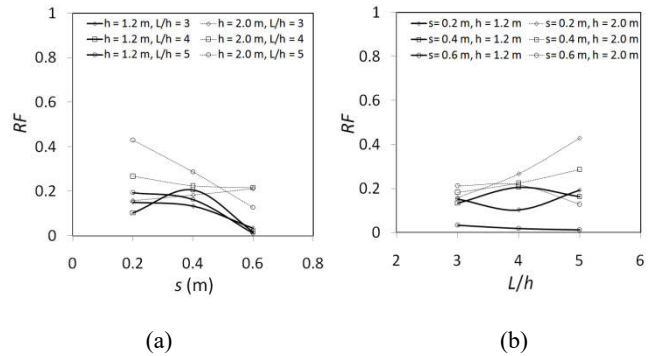


Figure 6 Variation of  $RF$  with (a) Reinforcement spacing,  $s$  and (b)  $L/h$  ratio

5.4 Effect of interface friction between soil and geogrid

In order to study the significance of interface friction between the soil and geogrid, the FE simulations for the 2 m high GRS abutments are carried out with the assumption of frictionless interface between the soil and geogrid. The corresponding passive force curves are plotted in Figure 7. It can be observed from the figure that the passive forces on the GRS abutments with smooth geogrids are lesser than that of the GRS abutments with rough geogrids.

Among all the GRS abutment configurations, the closely spaced longer geogrids reduced the passive forces considerably. It is to be noted that as the number of geogrid layers decreases, the abutment exhibits a similar behaviour as that of the unreinforced abutment.

5.5 Deformation profile of GRS abutments

The displacement contours of the GRS and unreinforced abutments of height 1.2 m for a lateral push of 0.2 m into the soil are shown in Figure 8. The geogrids are shown in red colour with continuous thin lines. It is noted that the upward moving soil wedge tried to lift the geogrids along with it. The presence of geogrids in the backfill soil effected the discontinuities to form in the displacement contours. The soil above the bottom geogrid undergoes more lateral displacement than that lie below the bottom geogrid. However, the uplift of the geogrid is constrained by the geogrid embedded in the stationary portion of the backfill soil which is on the other side of the moving soil wedge. The stationary backfill soil holds the geogrid layers from

getting pulled away from the soil along with the upward moving soil by mobilising the frictional resistance along their interfaces.

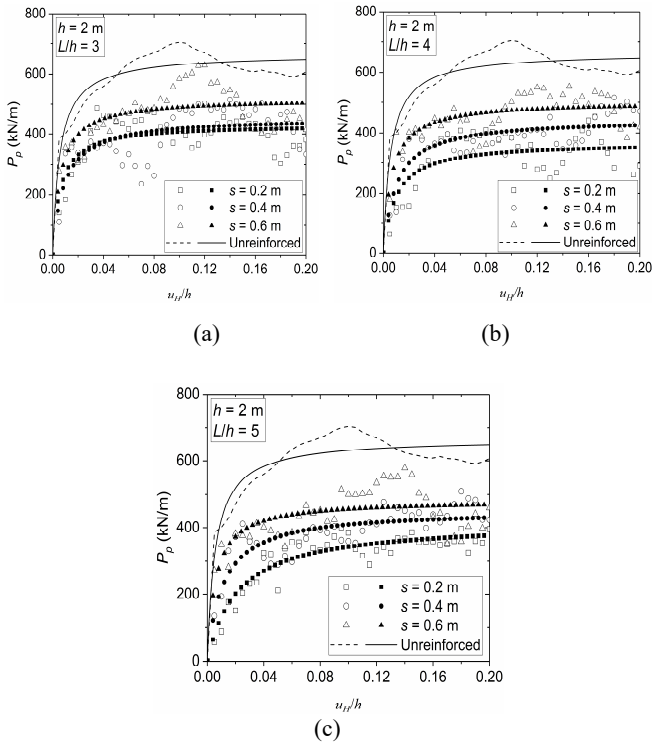


Figure 7  $P_p$  vs  $u_H$  for frictionless geogrids

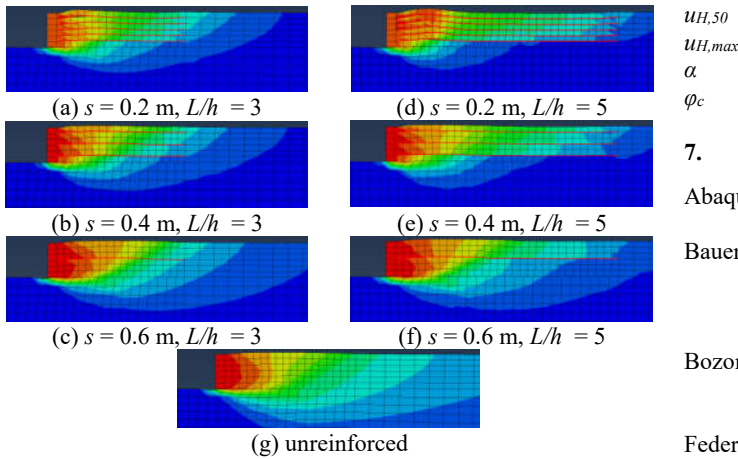


Figure 8 Displacement contours of the GRS and unreinforced abutments of  $h = 1.2$  m at  $u_H = 0.3$  m

## 6. CONCLUSIONS

The results of the FE simulations of lateral passive push on the GRS abutments are presented in the paper. The soil behaviour has been modelled with a continuum mechanics based hypoplastic constitutive model with intergranular strain concept. The user material subroutine VUMAT is developed exclusively to model the soil behaviour in Abaqus 6.12 Explicit solver. The GRS abutments of eighteen different configurations involving three different geogrid spacings ( $s$ ) and three different geogrid length to abutment height ( $L/h$ ) ratios are modelled and analysed to bring out the effect of spacing and  $L/h$  on the passive force of the GRS abutments.

The HFD plots for the unreinforced and GRS bridge abutments are developed from the FE results. The GRS abutments show

considerable decrease in the value of the initial tangent stiffness ( $K_i$ ) and maximum passive force ( $P_{pmax}$ ). Based on the results of the present study, the maximum reduction factor for  $K_i$  is 0.84. The reduction in passive force is the maximum for the GRS abutments with closely spaced longer geogrids. The results of the present study have relevance in the context of equivalent seismic loading on the bridge abutments for the evaluation of lateral force-displacement response. The evaluation of the passive capacity of the GRS bridge abutment-wall systems under cyclic and seismic loadings is currently underway.

## Notations

$C_u$	Uniformity coefficient of soil
$d_{50}$	Mean grain size of soil
$e_{c0}$	Void ratio identical to the maximum void ratio $e_{max}$ or with critical $e_c$ for continued granular flow at vanishing pressure
$e_{d0}$	Void ratio identical to the conventional minimum void ratio $e_{min}$ .
$e_{i0}$	Maximum possible void ratio at zero pressure; $e_{i0} = 1.1 e_{c0}$ can be often assumed.
$h$	Height of the GRS abutment
$h_s$	Granular hardness
$RF$	Reduction Factor
$K_{50}$	average abutment stiffness
$K_i$	Initial tangent stiffness of the abutment-wall system
$L$	Length of the geogrid reinforcement
$n$	an exponent appearing in the power law for proportional compression
$P_p$	Passive force generated
$P_{pmax, unrein}$	Maximum passive force of unreinforced abutment
$P_{pmax, GRS}$	Maximum passive force of GRS abutment
$s$	Spacing of the geogrid reinforcement
$u_H$	Uniform horizontal lateral push on the abutment wall
$u_{H,50}$	lateral displacement of the abutment wall at $P_{pmax} / 2$
$u_{H,max}$	lateral displacement of the abutment wall at $P_{pmax}$
$\alpha$	An exponent that can be estimated from $d_{50}$ and $C_u$
$\varphi_c$	Critical friction angle of soil

## 7. REFERENCES

Abaqus 6.12-3. (2012) Abaqus theory manual and user's manual. Providence, RI: Dassault Systèmes Simulia Corp.

Bauer, E. and Wu, W. (1993) "A hypoplastic model for granular soils under cyclic loading". In: D. Kolymbas, ed. Modern Approaches to Plasticity. Amsterdam: Elsevier Science Publishers B. V., pp. 247-258.

Bozorgzadeh, A. (2007) Effect of structure backfill on stiffness and capacity of bridge abutments. Thesis (PhD). University of California, San Diego.

Federal Emergency Management Agency (FEMA). (2000) Prestandard and commentary for the seismic rehabilitation of buildings. Washington, D.C: FEMA, FEMA-356.

Fredrickson, A., Rollins, K. M. and Nicks, J. (2017) "Passive Force-Deflection Behaviour of Geosynthetic-Reinforced Soil Backfill Based on Large-Scale Tests". Geotechnical Frontiers 2017, GSP 278, pp. 23-32.

Herle, I. and Gudehus, G. (1999) "Determination of parameters of a hypoplastic constitutive model from properties of grain assemblies". Mechanics of Cohesive Frictional Materials, 4, pp. 461-486.

Kolymbas, D. (2000) Introduction to Hypoplasticity. Rotterdam: A. A. Balkema.

Lemmitzer, A., Ahlberg, E. R., Nigbor, R. L., Shamsabadi, A., Wallace, J. W., and Stewart, J. P. (2009) "Lateral performance of full-scale bridge abutment wall with granular backfill". Journal of Geotechnical and Geoenvironmental Engineering, 135, pp. 506-514.

- Niemunis, A. and Herle, I. (1997) "Hypoplastic model for cohesionless soils with elastic strain range". *Mechanics of Cohesive Frictional Materials*, 2, pp. 279-299.
- Rollins, K. M. and Jessee, S. J. (2013) "Passive force-deflection curves for skewed abutments". *Journal of Bridge Engineering*, 18, pp. 1086-1094.
- Shamsabadi, A., Rollins, K. M. and Kapuskar, M. (2007) "Nonlinear soil–abutment–bridge structure interaction for seismic performance-based design". *Journal of Geotechnical and Geoenvironmental Engineering*, 133, pp. 707-720.
- Shamsabadi, A., Khalili-Tehrani, P., Stewart J. P. and Taciroglu, E. (2010) "Validated simulation models for lateral response of bridge abutments with typical backfills". *Journal of Bridge Engineering*, 15, pp. 302-311.
- Stewart, J. P., Taciroglu, E., Wallace, J. W., Ahlberg, E. R., Lemnitzer, A., Rha, C., Tehrani, P., Keowen, S., Nigbor, R. L., and Salamanca, A. (2007) Full scale cyclic testing of foundation support systems for highway bridges. Part II: Abutment backwalls. Los Angeles: University of California, UCLA-SGEL 2007/02.
- von Wolffersdorff, P.-A. (1996) "A hypoplastic relation for granular materials with a predefined limit state surface". *Mechanics of Cohesive Frictional Materials*, 1, pp. 251–271.
- Wilson, P. R. (2009) Large scale passive force-displacement and dynamic earth pressure experiments and simulations. Thesis (PhD). University of California, San Diego.
- Wilson, P. and Elgamal, A. (2010) "Large-scale passive earth pressure load-displacement tests and numerical simulation". *Journal of Geotechnical and Geoenvironmental Engineering*, 136, pp. 1634-1643.
- Wu, J. T. H., Lee, K. Z. Z, Helwany, S. B., and Ketchart, K. (2006) Design and construction guidelines for geosynthetic-reinforced soil bridge abutments with a flexible facing. Washington D.C.: NCHRP, NCHRP-556.